An Improved Dirichlet-to-Neumann Map Method for Scattering by Circular Cylinders on a Lattice

Shichang She and Ya Yan Lu

Department of Mathematics, City University of Hong Kong, Kowloon, Hong Kong

A simple model for two-dimensional photonic crystal devices consists of finite number of possibly different circular cylinders centered on lattice points of a square or triangular lattice and surrounded by a homogeneous or layered background medium. The Dirichlet-to-Neumann (DtN) map method is a special method for analyzing the scattering of an incident wave by such a structure. It is more efficient than existing numerical or semi-analytic methods, such as the finite element method and the multipole method, since it takes advantage of the underlying lattice structure and the simple geometry of the unit cells. The DtN map of a unit cell is a relation between a wave field component and its normal derivative on the cell boundary, and it can be used to avoid further computation inside the unit cell. In this paper, an improved DtN map method is developed by constructing special DtN maps for boundary and corner unit cells using the method of fictitious sources.

OCIS codes: 290.4210, 050.1755, 000.4430

1. Introduction

In recent years, many photonic components and devices have been developed using photonic crystals (PhCs) to take advantage of the bandgap effect and unusual dispersion properties [1]. Although the principle of many devices can be illustrated by relatively simple designs obtained from physical intuitions or simple models, practical applications often require a systematic optimization based on rigorous numerical simulations. Due to the intentionally introduced defects, a PhC device is usually not periodic. Unlike band structure calculations that are performed on a unit cell, the propagation of light in a PhC device gives rise to a large boundary value problem involving many unit cells. Efficient and accurate numerical methods are needed to speed up the design and optimization process.

As a model for PhC devices, we consider ideal two-dimensional (2D) structures with a finite number of circular cylinders (dielectric rods or air holes) centered on lattice points of a

square or triangular lattice, where the cylinders at different locations can have different radii and different refractive indices. The medium outside the cylinders is homogeneous or layered (where each layer is homogeneous). To analyze the scattering of a given incident wave by such a multi-cylinder lattice structure, numerical or semi-analytic methods are needed. The finite-difference time-domain (FDTD) method [2] is extremely versatile and widely used, but it often requires long computation time, since a small mesh size is needed to resolve material interfaces where the index-contrast is often high, and a small time step is needed to maintain numerical stability. The finite element method (FEM) [3] is also very general, but it leads to large linear systems that are relatively expensive to solve. In the frequency domain, it is possible to develop more efficient computational methods by taking advantage of the geometric features. The multipole method (also called multipole expansion method, cylindrical wave expansion method, scattering-matrix method, multiple-scattering method) [4–10] is quite popular, it solves a system of equations for the coefficients of local cylindrical wave expansions around each cylinder, and it is usually more efficient than the general FDTD and FEM methods. The multipole method has been extended to multi-cylinder structures with a layered background medium involving one or more planar interfaces [11–15], but it becomes relatively complicated for these cases.

The Dirichlet-to-Neumann (DtN) map method [16–18] is a recently developed method for analyzing 2D PhC devices. It uses a cylindrical wave expansion in each unit cell to establish a relation (the so-called DtN map) between the wave field and its normal derivative on the cell boundary, then solves the wave fields on the boundaries of the unit cells only. The method presented in [16] deals with PhC devices connected by a few waveguides (as input and output ports) in an infinite background PhC. In particular, it makes use of rigorous boundary conditions to terminate semi-infinite PhC waveguides and obtain a finite computational domain. Compared with the multipole method, the DtN map method has the advantage of producing sparse and better-conditioned linear systems that are much easier to solve. The DtN map method can also be used to analyze PhC devices involving finite number of cylinders, but a different domain truncation technique is needed. The approach used in [18] is to surround the cylinders by one layer of empty unit cells and construct special DtN maps for the boundary and corner unit cells using expansions in plane waves.

In this paper, we present an improved DtN map method for PhC devices or any general 2D multi-cylinder lattice structures with a finite number of circular cylinders. The DtN maps constructed using plane waves [18] seem to have limited accuracy. We construct more accurate DtN maps for boundary and corner unit cells based on the method of fictitious sources [19], and illustrate the DtN map method using a number of examples including a structure with a layered background.

2. The DtN map method

For 2D structures that are invariant in the z direction, if the electromagnetic field is also independent of z, then it can be decomposed as the E and H polarizations. For the E polarization, the z component of the electric field, denoted by u in this paper, satisfies the Helmholtz equation

$$\frac{\partial^2 u}{\partial x^2} + \frac{\partial^2 u}{\partial y^2} + k_0^2 n^2(\boldsymbol{r})\, u = 0, \tag{1}$$

where $\boldsymbol{r} = (x, y)$, k_0 is the free space wavenumber, and $n(\boldsymbol{r})$ is the refractive index function. The time dependence is assumed to be $e^{-i\omega t}$ for an angular frequency ω. For the H polarization, the governing equation is

$$\frac{\partial}{\partial x}\left[\frac{1}{n^2(\boldsymbol{r})}\frac{\partial u}{\partial x}\right] + \frac{\partial}{\partial y}\left[\frac{1}{n^2(\boldsymbol{r})}\frac{\partial u}{\partial y}\right] + k_0^2\, u = 0, \tag{2}$$

where u is the z component of the magnetic field. For a multi-cylinder structure involving a finite number of non-overlapping circular cylinders surrounded by a homogeneous medium with a refractive index n_0, a standard problem is to calculate the scattered wave $u^{(s)}$ for a given incident wave $u^{(i)}$, such that the total field $u = u^{(i)} + u^{(s)}$ satisfies Eq. (1) or Eq. (2). Typically, the incident wave is a plane wave given by

$$u^{(i)}(\boldsymbol{r}) = \exp[i(\alpha_0 x + \beta_0 y)] \tag{3}$$

with a wave vector (α_0, β_0) satisfying $\alpha_0^2 + \beta_0^2 = k_0^2 n_0^2$.

The basic idea of the DtN map method is to take advantage of the many identical unit cells by computing the DtN maps of the unit cells. The DtN map of a unit cell is an operator that maps the wave field to its normal derivative on the cell boundary. The method was first proposed for computing transmission and reflection spectra of finite number of arrays of cylinders [20], and it has been used to analyze many different PhC structures [21–25]. For 2D PhC devices in an infinite PhC with a few waveguides (as input and output ports) extending to infinity, a rigorous boundary condition for terminating PhC waveguides was developed [16]. If a device is embedded in a finite PhC and surrounded by a homogeneous or layered medium, a different domain truncation technique is needed. One approach is to truncate the domain by including only one layer of empty unit cells in the surrounding homogeneous media, and use special DtN maps for the boundary and corner unit cells. In [18], the boundary and corner DtN maps are constructed using plane waves, but the accuracy is limited. In the following, we construct new DtN maps for the boundary and corner unit cells based on the method of fictitious sources and show improved accuracy in numerical examples.

To illustrate the DtN map method for finite multi-cylinder lattice structures, we consider an example shown in Fig. 1(a). The structure consists of $N = 10$ identical cylinders, and

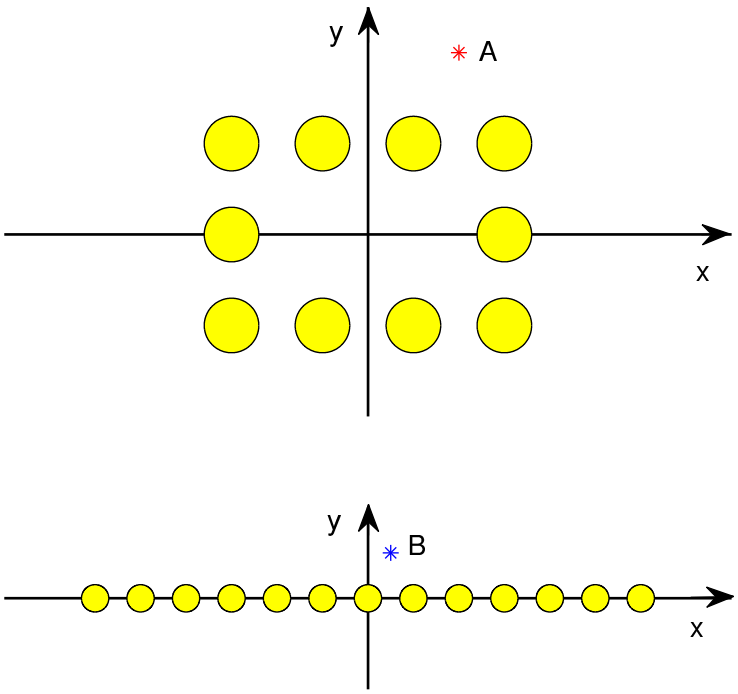

Fig. 1. (a) Ten cylinders in a rectangular loop; (b) Thirteen cylinders in a row.

the centers of these cylinders are lattice points of a square lattice with lattice constant a. In the DtN map method, the xy plane is truncated to a rectangular region containing 6×5 unit cells as shown in Fig. 2. If the lower-left corner is (x_0, y_0), then the unit cell Ω_{jk} is the square given by $x_{j-1} < x < x_j$ and $y_{k-1} < y < y_k$, where $x_j = x_0 + ja$, $y_k = y_0 + ka$, etc. We use v_{jk} and h_{jk} to denote u on vertical and horizontal edges, respectively. More precisely, $v_{jk} = u(x_j, y)$ for $y_{k-1} < y < y_k$ and $h_{jk} = u(x, y_k)$ for $x_{j-1} < x < x_j$.

For an interior unit cell Ω_{jk} $(2 \le j \le 5,\ 2 \le k \le 4)$, its DtN map $\mathbf{\Lambda}_{jk}$ satisfies

$$\mathbf{\Lambda}_{jk} \begin{bmatrix} v_{j-1,k} \\ h_{j,k-1} \\ v_{jk} \\ h_{jk} \end{bmatrix} = \begin{bmatrix} \partial_x v_{j-1,k} \\ \partial_y h_{j,k-1} \\ \partial_x v_{jk} \\ \partial_y h_{jk} \end{bmatrix}, \tag{4}$$

where $\partial_x v_{jk}$ denotes $\partial_x u$ evaluated on the same edge as v_{jk}, etc. For the boundary and corner unit cells, the DtN maps are defined for the scattered field $u^{(s)}$ and they do not involve the edges on the boundary of the truncated domain. Therefore, the DtN map of a boundary unit cell involves three interior edges. For example, the DtN map $\mathbf{\Lambda}_{21}$ of the boundary unit cell

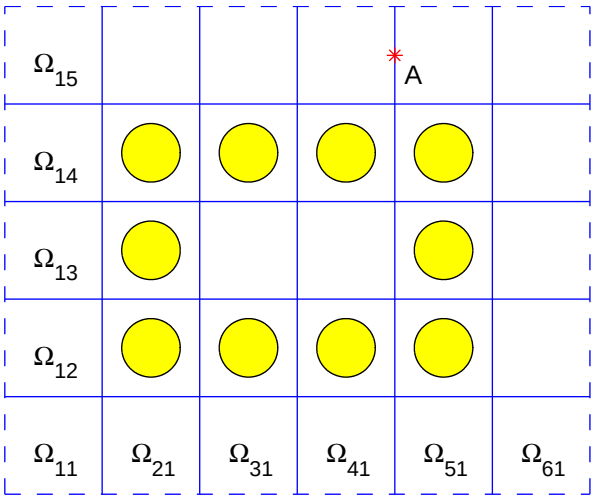

Fig. 2. The truncated domain and unit cells for Example 1 shown in Fig. 1(a).

Ω_{21} satisfies

$$\mathbf{\Lambda}_{21} \begin{bmatrix} v_{11}^{(s)} \\ v_{21}^{(s)} \\ h_{21}^{(s)} \end{bmatrix} = \begin{bmatrix} \partial_x v_{11}^{(s)} \\ \partial_x v_{21}^{(s)} \\ \partial_y h_{21}^{(s)} \end{bmatrix}. \tag{5}$$

The DtN map of a corner unit cell (Ω_{11}, Ω_{61}, Ω_{15} or Ω_{65} in Fig. 2) involves only two interior edges. For Ω_{11}, its DtN map $\mathbf{\Lambda}_{11}$ satisfies

$$\mathbf{\Lambda}_{11} \begin{bmatrix} v_{11}^{(s)} \\ h_{11}^{(s)} \end{bmatrix} = \begin{bmatrix} \partial_x v_{11}^{(s)} \\ \partial_y h_{11}^{(s)} \end{bmatrix}. \tag{6}$$

In the discrete case, if each edge of the interior unit cells is sampled by p points and each edge in the boundary layer is sampled by p_0 points, then the interior, boundary and corner DtN maps are approximated by $(4p) \times (4p)$, $(p+2p_0) \times (p+2p_0)$ and $(2p_0) \times (2p_0)$ matrices, respectively. We note that p_0 may be different from p.

Based on the DtN maps, we can set up a system of equations for all interior edges [18]. For each interior edge, an equation is obtained by equating the normal derivative (x or y derivative for a vertical or horizontal edge, respectively) of the wave field evaluated by the DtN maps of the two neighboring unit cells. The system is for the total field on the edges of the interior unit cells and the scattered field on the edges in the boundary layer. Therefore, we need to substitute $u^{(s)}$ by $u - u^{(i)}$ on one edge in the DtN map of a boundary unit cell. For Ω_{21}, we need to replace $h_{21}^{(s)}$ by $h_{21} - h_{21}^{(i)}$. The final system is sparse, since each equation involves at most seven edges of two neighboring unit cells. This is a favorable feature of

the DtN map method. In the multipole method, the linear system of equations has a dense coefficient matrix [6, 9].

3. Construction of DtN maps

For an interior unit cell, the DtN map can be easily constructed by expanding the wave field in cylindrical waves [20]. For boundary and corner unit cells, plane waves have been used to construct the DtN maps [18], but the accuracy seems to be limited. In the following, we use the method of fictitious sources [19] to construct the DtN maps. Consider a unit cell $\Omega^{(b)}$ in the top boundary layer, we approximate the scattered wave $u^{(s)}$ in $\Omega^{(b)}$ by the wave field generated by $p + 2p_0$ point sources located below the unit cell with unknown coefficients, where p and p_0 are positive integers. If the sources are located at $\boldsymbol{s}_j$ for $1 \le j \le p + 2p_0$, then

$$u^{(s)}(\boldsymbol{r}) \approx \sum_{j=1}^{p+2p_0} c_j H_0^{(1)}(k_0 n_0 |\boldsymbol{r} - \boldsymbol{s}_j|), \quad \boldsymbol{r} \in \Omega^{(b)}. \tag{7}$$

Next, we choose p_0, p and p_0 points on the left, lower and right edges of $\Omega^{(b)}$ respectively, and evaluate $u^{(s)}$ and its normal derivative at these points by (7). The DtN map of $\Omega^{(b)}$ is then obtained by eliminating the coefficients c_j ($1 \le j \le p + 2p_0$). Notice that the approximate DtN map satisfies (5) at these $p + 2p_0$ points exactly for $u^{(s)}$ given in (7).

The key question is how to distribute the point sources. An optimal distribution is difficult to define, is perhaps solution-dependent, and is not necessary for our purpose. Instead, we simply choose a curve below the unit cell $\Omega^{(b)}$ and distribute the sources uniformly on it. We consider three cases as shown in Fig. 3(a-c), where the curves are a horizontal line, a U-shaped curve and a V-shaped curve, respectively. Even for these simple curves, we need to choose geometric parameters such as the vertical distance to the unit cell, the length of the horizontal line, the width and height of the U-curve, the length and the angle of the V-curve. Our choice for these geometric parameters are depicted in Fig. 3. To find these parameters, we minimize the maximum relative errors of the normal derivatives computed by the DtN map for some testing functions. In a coordinate system where the center of $\Omega^{(b)}$ is the origin, we choose testing functions as multipoles located below the unit cell, that is,

$$U_m(\boldsymbol{r}; \boldsymbol{t}) = H_m^{(1)}(k_0 n_0 |\boldsymbol{r} - \boldsymbol{t}|) e^{im\theta(\boldsymbol{r}-\boldsymbol{t})} \tag{8}$$

where $\boldsymbol{t}$ is the center of the multipole, m is its order, and $\theta(\boldsymbol{r} - \boldsymbol{t})$ is the polar angle of $\boldsymbol{r} - \boldsymbol{t}$. To compare the three different constructions, we show the maximum relative errors on the three edges of $\Omega^{(b)}$ for a few testing functions and for $p = 11$ and $p_0 = 9$. The results are listed in Table 1. It is observed that the DtN map constructed from the U-curve has the highest overall accuracy. Comparing with the DtN map constructed using plane waves [18]

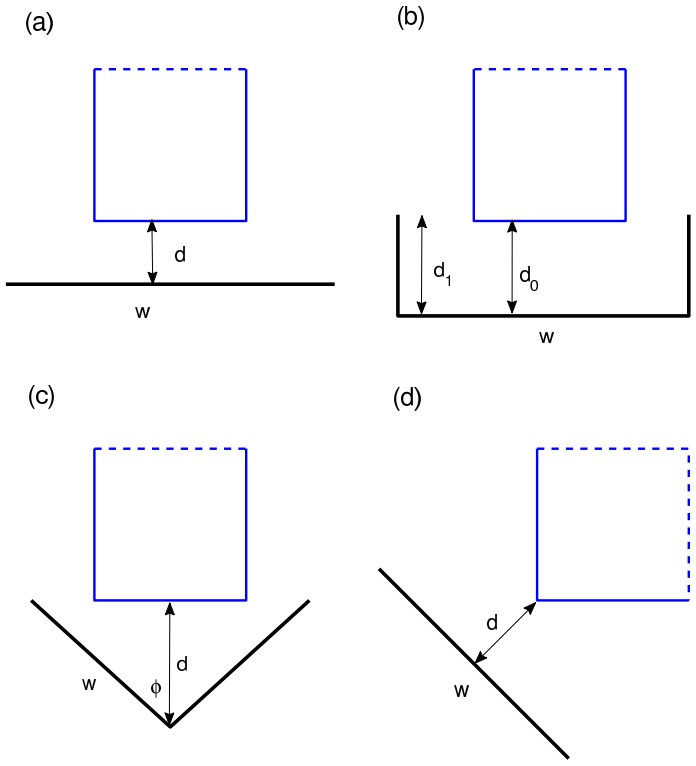

Fig. 3. For a boundary unit cell, sources are located on a horizontal line (a), a U-curve (b), or a V-curve (c). For a corner unit cell, sources are located on a line (d). Geometric parameters are: (a) $d = 1.3a$, $w = 4.8a$; (b) $d_0 = 1.6a$, $d_1 = a$, $w = 2.25a$; (c) $d = 1.28a$, $w = 1.8a$, $\phi = 84°$; (d) $d = 2a$, $w = 2a$.

for which the relative error is about 10^{-3} for the two zeroth order testing functions, these new boundary DtN maps are clearly more accurate.

The DtN map of a corner unit cell $\Omega^{(c)}$ can be constructed similarly by the method of fictitious sources. We approximate the scattered field in $\Omega^{(c)}$ by a sum of $2p_0$ sources located at $\boldsymbol{s}_j$ for $1 \le j \le 2p_0$, i.e.,

$$u^{(s)}(\boldsymbol{r}) \approx \sum_{j=1}^{2p_0} c_j H_0^{(1)}(k_0 n_0 |\boldsymbol{r} - \boldsymbol{s}_j|), \quad \boldsymbol{r} \in \Omega^{(c)}, \tag{9}$$

then evaluate $u^{(s)}$ and its normal derivative on the two interior edges of $\Omega^{(c)}$, and finally find the DtN map by eliminating the coefficients c_j $(1 \le j \le 2p_0)$. The sources are located on a line as shown in Fig. 3(d) when $\Omega^{(c)}$ is the top-right corner unit cell.

m	$\boldsymbol{t}$	horizontal line	U-curve	V-curve
5	$(-60a, -a)$	0.052689	0.0310944	0.051555
5	$(0, -a)$	0.064214	0.0106649	0.009561
5	$(-a, -a)$	0.007494	0.0002250	0.000284
5	$(-30a, -30a)$	0.000385	0.0002906	0.000153
0	$(0, -a)$	0.000011	0.0000031	0.000003
0	$(-a, -a)$	0.000282	0.0000003	0.000002

Table 1. Maximum relative errors of normal derivatives of test functions on the edges of a boundary unit cell, where m and $\boldsymbol{t}$ are the order and the center of the multipole testing function given in (8).

4. Numerical examples

To illustrate the performance of the improved DtN map method, we consider two examples. The first example consists of $N = 10$ identical cylinders as shown in Fig. 1(a). The centers of these cylinders are lattice points of a square lattice with lattice constant a. The refractive index and the radius of the cylinders are $n = 2$ and $R = 0.3a$, respectively. The surrounding medium is air (thus $n_0 = 1$). The incident wave is a plane wave with a wave vector forming a 45° with the y axis, that is

$$(\alpha_0, \beta_0) = k_0 n_0 \left(\frac{1}{\sqrt{2}}, -\frac{1}{\sqrt{2}} \right). \tag{10}$$

The problem is considered for the E polarization and a free space wavelength $\lambda = 1.25a$ (i.e., $k_0 = 1.6\pi/a$). In particular, we calculate the scattered wave at $(a, 2a)$, i.e., point A in Fig. 1(a). In Table 2, we list the numerical solutions obtained by the improved and original DtN map methods (denoted by DtN(i) and DtN(o), respectively), using the truncated domain shown in Fig. 2. For the improved method, the DtN maps of the boundary unit cells are constructed by fictitious sources distributed on the U-curve, and the results are given for a few values of p and a fixed $p_0 = 9$. For the original method, we use the parameter $\alpha_* = 5k_0 n_0$ for truncating plane wave expansions in the construction of boundary and corner DtN maps [18]. To validate the improved DtN map method, we also solve this problem by the multipole method and a second order FEM with triangular elements. The multipole method gives rise to a dense linear system for $(2m_* + 1)N$ expansion coefficients, where m_* is the truncation order and N is the total number of cylinders. A brief summary of the multipole method is given in the Appendix. In Table 2, the multipole and FEM solutions are listed for a few values of m_* and N_f respectively, where N_f is the total number of nodes (i.e. the size of the

Method	$u^{(s)}(a, 2a)$	R.E.
DtN(i), $p = 10$	0.09017 - 0.35358i	0.00047
DtN(i), $p = 11$	0.09048 - 0.35331i	0.00066
DtN(i), $p = 12$	0.09030 - 0.35349i	0.00007
DtN(i), $p = 13$	0.09019 - 0.35360i	0.00047
DtN(i), $p = 14$	0.09014 - 0.35335i	0.00051
DtN(o), $p = 12$	0.08818 - 0.35428i	0.0062
DtN(o), $p = 13$	0.08822 - 0.35287i	0.0059
DtN(o), $p = 14$	0.08990 - 0.35465i	0.0034
DtN(o), $p = 15$	0.08953 - 0.35345i	0.0021
Multipole, $m_* = 4$	0.090288 - 0.353465i	–
Multipole, $m_* = 5$	0.090295 - 0.353466i	–
Multipole, $m_* = 6$	0.090295 - 0.353465i	–
FEM, $N_f = 32244$	0.090947 - 0.353206i	–
FEM, $N_f = 129167$	0.090291 - 0.353464i	–
FEM, $N_f = 515375$	0.090295 - 0.353465i	–

Table 2. Example 1: $u^{(s)}$ at point A computed by the improved and original DtN map methods (denoted as DtN(i) and DtN(o) respectively), the multipole method and the FEM. The relative errors (R.E.) in the last column are calculated using the reference solution $u^{(s)}(a, 2a) = 0.090295 - 0.353465i$.

linear system). From the multipole and FEM results, we obtain a reference solution with six correct digits $u^{(s)}(a, 2a) \approx 0.090295 - 0.353465i$, and it is used to calculate the relative errors for solutions obtained by the DtN map methods. From the relative errors listed in the last column of Table 2, it is clear that the improved DtN map method is more accurate than the original method. In particular, the most accurate solution of the improved DtN map method is obtained with $p = 12$.

The second example consists of $N = 13$ cylinders in a row as shown in Fig. 1(b). The cylinders are assumed to have the same refractive index ($n = 2$) and the same radius ($R = 0.3a$) as in the first example, where a is the center-to-center distance between nearby cylinders. The surrounding medium and the incident wave are also identical to those of the first example. For this problem, we calculate the scattered wave at $(0.5a, a)$, i.e., point B in Fig. 1(b), for the E polarization. For the DtN map methods, we surround the 13 cylinders by a layer of empty unit cells, thus the truncated domain is a rectangular region with 15×3 unit cells. The

numerical solutions are listed in Table 3. The multipole and FEM results give us a reference

Method	$u^{(s)}(0.5a, a)$	R.E.
DtN(i), $p = 11$	-0.0365 + 0.1039i	0.0075
DtN(i), $p = 12$	-0.0363 + 0.1042i	0.0044
DtN(i), $p = 13$	-0.0363 + 0.1042i	0.0042
DtN(i), $p = 14$	-0.0365 + 0.1041i	0.0059
DtN(o), $p = 11$	-0.0470 + 0.0873i	0.185
DtN(o), $p = 12$	-0.0404 + 0.1070i	0.044
DtN(o), $p = 13$	-0.0375 + 0.1053i	0.013
DtN(o), $p = 14$	-0.0359 + 0.1032i	0.014
Multipole, $m_* = 3$	-0.03623 + 0.10474i	–
Multipole, $m_* = 4$	-0.03620 + 0.10468i	–
Multipole, $m_* = 5$	-0.03619 + 0.10468i	–
FEM, $N_f = 91944$	-0.03622 + 0.10472i	–
FEM, $N_f = 366343$	-0.03613 + 0.10470i	–
FEM, $N_f = 1453169$	-0.03619 + 0.10468i	–

Table 3. Example 2: $u^{(s)}$ at point B computed by the improved and original DtN map methods, the multipole method and the FEM. The relative errors (R.E.) in the last column are calculated based on the reference solution $u^{(s)}(0.5a, a) \approx -0.03619 + 0.10468i$.

solution $u^{(s)}(0.5a, a) \approx -0.03619 + 0.10468i$, and it is used to calculate the relative errors for the DtN solutions. For the improved DtN map method, the results in Table 3 are obtained for a fixed $p_0 = 7$ and different values of p. Although the accuracy is still somewhat limited, it is clear that the improved DtN map method gives more accurate results than the original method.

5. Cylinders embedded in a slab

While the multipole method was originally developed for a set of cylinders in a homogeneous medium, it has been extended to cases where the background is a layered medium with one or more planar interfaces [11–15]. In these cases, the method becomes quite complicated, since it is necessary to consider the plane-wave spectra of cylindrical waves, to analyze the transmission and reflection of cylindrical waves by planar interfaces, and to take care of the multiple scattering between all planar interfaces and cylinders. A generalized method of

images was introduced in [14] to simplify the problem, but it has its own limitations related to the convergence of a Fourier series in the complex plane. On the other hand, the DtN map method can be used to analyze structures with a layered background without any difficulty.

To illustrate the DtN map method, we consider the structure shown in Fig. 4. It is a

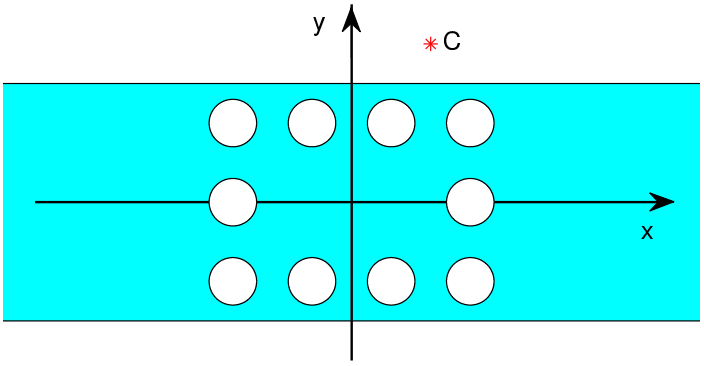

Fig. 4. A dielectric slab with ten holes forming a rectangular loop.

dielectric slab with 10 air holes arranged as a rectangular loop. The refractive index of the slab is $n_1 = 1.5$, the thickness of the slab is $3a$, and the centers of the holes are located at some lattice points of a square lattice with lattice constant a. The medium above and below the slab is air ($n_0 = 1$). As before, we consider an incident plane wave given by Eq. (3) for free space wavenumber $k_0 = 1.6\pi/a$. For such a problem with a layered background, the scattered field $u^{(s)}$ should be defined such that the total field is

$$u = u^* + u^{(s)}, \tag{11}$$

where u^* is the solution excited by the incident wave for the slab without the holes. More precisely, we have

$$u^*(x,y) = \begin{cases} u^{(i)} + Re^{i(\alpha_0 x + \beta_0 y)}, & \text{above the slab,} \\ [C_1 e^{i\beta_1 y} + C_2 e^{-i\beta_1 y}]e^{i\alpha_0 x}, & \text{within the slab,} \\ Te^{i(\alpha_0 x - \beta_0 y)}, & \text{below the slab,} \end{cases} \tag{12}$$

where $\beta_1 = \sqrt{k_0^2 n_1^2 - \alpha_0^2}$. The unknown coefficients R, T, C_1 and C_2, where R and T are the reflection and transmission coefficients, can be determined from the continuity conditions of u^* and $\partial_y u^*$ on the boundaries of the slab.

To use the DtN map method, we truncate the xy plane to a $(6a) \times (5a)$ rectangle, similar to the one shown in Fig. 2. The rectangle consists of 30 square unit cells of size $a \times a$. They

include homogeneous unit cells of refractive index n_1 or n_0, and unit cells with a circular air hole. The corner unit cells and boundary unit cells in the top and bottom rows have refractive index n_0, and the left and right boundary unit cells in the slab have refractive index n_1. The DtN maps of all these unit cells can be constructed by the method described in section 3. In particular, the boundary DtN maps are constructed using the U-curve source distribution. For all corner and boundary unit cells, the DtN maps are developed for the scattered wave. Based on these DtN maps, we can set up a system of equations for u or $u^{(s)}$ on the 49 edges of the unit cells. Notice that $u^{(s)}$ is used on edges that separate boundary and/or corner unit cells. Numerical results for $u^{(s)}$ at point C are listed in Table 4. For comparison, we

Method	$u^{(s)}$ at point C	R.E.
DtN(i), $p = 9$	-0.06183 - 0.30986i	0.00038
DtN(i), $p = 10$	-0.06167 - 0.30995i	0.00039
DtN(i), $p = 11$	-0.06164 - 0.30996i	0.00049
DtN(i), $p = 12$	-0.06171 - 0.30994i	0.00028
DtN(i), $p = 13$	-0.06168 - 0.30997i	0.00036
DtN(i), $p = 14$	-0.06170 - 0.30987i	0.00043
DtN(i), $p = 15$	-0.06169 - 0.30989i	0.00042
FEM, $N_f = 32244$	-0.062259 - 0.310729i	–
FEM, $N_f = 129167$	-0.061793 - 0.309973i	–
FEM, $N_f = 515375$	-0.061793 - 0.309974i	–

Table 4. Numerical solutions for the dielectric slab with ten holes. The DtN results are obtained with $p_0 = 9$. The FEM results are obtained on a triangular mesh with N_f nodes. Relative errors are calculated based on the most accurate FEM solution.

also list three solutions obtained by a second order FEM with triangular elements. Using the most accurate FEM solution, we calculate approximate relative errors for other numerical solutions. From the last column of Table 4, we observe that the relative errors of the solutions obtained by the DtN map method are less than 0.0005 for all p satisfying $9 \leq p \leq 15$. Same as in the first example in section 4, the most accurate DtN map solution is obtained with $p = 12$.

The numerical results in section 4 and this section are given for the E polarization only. The method is certainly applicable to the H polarization. The difference is mainly in the construction of DtN maps for interior unit cells. We concentrate on the E polarization, since the main purpose of this work is to reduce the error in the boundary and corner unit cells.

For the H polarization, accurate DtN maps for interior unit cells can be easily constructed, see for example [26].

6. Conclusions

In this paper, we developed an improved DtN map method for two-dimensional structures involving finite number of possibly different circular cylinders centered on lattice points of a square lattice. The DtN map method was first proposed for PhC devices in an infinite background PhC [16,17] and latter extended to PhC devices in a finite PhC based on special DtN maps for boundary and corner unit cells [18]. The improved DtN map method developed in this paper uses the method of fictitious sources to construct the DtN maps for the boundary and corner unit cells, and produces more accurate solutions. We also extend the DtN map method to structures where the cylinders are surrounded by a multilayer medium.

For structures concerned here, general numerical methods such as the finite element method are certainly applicable, but the multipole method [4–9] is more competitive. The multipole method produces a linear system with a dense coefficient matrix. The DtN map method gives a linear system of similar size, but the coefficient matrix is sparse. Moreover, the extension of the multipole method to structures with a layered background is somewhat complicated [11–15], but the same extension of the DtN map method requires very little modification. Of course, the multipole method is applicable to arbitrary configurations of the cylinders, while the DtN map method requires that the centers of the cylinders coincide with lattice points of a lattice. Nevertheless, for applications in modeling PhC devices, a natural lattice structure exists and the DtN map method can be highly useful.

Acknowledgments

This research was partially supported by a grant from the Research Grants Council of Hong Kong Special Administrative Region, China (Project No. CityU 102411).

Appendix

The multipole method is a well-established method for analyzing the scattering of an incident wave by canonical scatterers such as cylinders and spheres [9]. For a finite multi-cylinder structure with N circular cylinders centered at $\boldsymbol{c}_l$ $(1 \le l \le N)$, the scattered wave outside the cylinders can be written as

$$u^{(s)}(\boldsymbol{r}) = \sum_{l=1}^{N} \sum_{m=-\infty}^{\infty} b_{lm} H_m^{(1)}(k_0 n_0 r_l) e^{im\theta_l}, \tag{13}$$

where $\boldsymbol{r} = (x, y)$, $\{r_l, \theta_l\}$ are the polar coordinates of $\boldsymbol{r} - \boldsymbol{c}_l$, and $H_m^{(1)}$ is a Hankel function of the first kind. Assuming that the lth cylinder has a radius R_l and a refractive index n_l,

the multipole method gives the following linear system for the unknown coefficients $\{b_{lm}\}$:

$$\boldsymbol{A}\begin{bmatrix}\boldsymbol{b}_1\\ \boldsymbol{b}_2\\ \vdots\\ \boldsymbol{b}_N\end{bmatrix} = \begin{bmatrix}\boldsymbol{I} & -\boldsymbol{S}_1\boldsymbol{T}_{12} & -\boldsymbol{S}_1\boldsymbol{T}_{13} & \cdots\\ -\boldsymbol{S}_2\boldsymbol{T}_{21} & \boldsymbol{I} & -\boldsymbol{S}_2\boldsymbol{T}_{23} & \cdots\\ -\boldsymbol{S}_3\boldsymbol{T}_{31} & -\boldsymbol{S}_3\boldsymbol{T}_{32} & \boldsymbol{I} & \cdots\\ \vdots & \vdots & \vdots & \ddots\end{bmatrix}\begin{bmatrix}\boldsymbol{b}_1\\ \boldsymbol{b}_2\\ \vdots\\ \boldsymbol{b}_N\end{bmatrix} = \begin{bmatrix}\boldsymbol{f}_1\\ \boldsymbol{f}_2\\ \vdots\\ \boldsymbol{f}_N\end{bmatrix}, \tag{14}$$

where $\boldsymbol{b}_l$ is the infinite column vector of b_{lm} for all m, $\boldsymbol{f}_l$ is an infinite column vector related to the incident wave $u^{(i)}$, $\boldsymbol{I}$ is the identity matrix, $\boldsymbol{S}_l$ is an infinite diagonal matrix and $\boldsymbol{T}_{lj}$ is an infinite matrix. The (m,q) entry of $\boldsymbol{T}_{lj}$ is

$$(\boldsymbol{T}_{lj})_{mq} = H^{(1)}_{m-q}(k_0 n_0 r_l^j)\exp[i(q-m)\theta_l^j],$$

where $\{r_l^j, \theta_l^j\}$ are the polar coordinates of $\mathbf{c}_j - \mathbf{c}_l$. For the E polarization, the (m,m) entry of $\boldsymbol{S}_l$ is

$$(\boldsymbol{S}_l)_{mm} = \frac{n_l J_m(\xi)J'_m(\eta) - n_0 J_m(\eta)J'_m(\xi)}{-n_l H^{(1)}_m(\xi)J'_m(\eta) + n_0 J_m(\eta)H^{(1)'}_m(\xi)},$$

where $\xi = k_0 n_0 R_l$ and $\eta = k_0 n_l R_l$. For the H polarization, n_0 and n_l should be switched in the above formula for $(\boldsymbol{S}_l)_{mm}$. If the incident wave is a plane wave with a wave vector (α_0, β_0), then $\boldsymbol{f}_l = \boldsymbol{S}_l\boldsymbol{q}_l$, where $\boldsymbol{q}_l$ is column vector of

$$q_{lm} = i^m \exp[ik_0 n_0 r^l \cos(\theta^l - \theta^{(i)}) - im\theta^{(i)}]$$

for all m, $\{r^l, \theta^l\}$ are the polar coordinates of $\boldsymbol{c}_l$, $\theta^{(i)}$ is the angle of incidence such that $\alpha_0 = k_0 n_0 \cos\theta^{(i)}$ and $\beta_0 = k_0 n_0 \sin\theta^{(i)}$. More details can be found in Refs. [6] and [9].

For actual calculations, the infinite system (14) must be truncated. If we truncate m to $|m| \le m_*$ for some integer m_*, then $\boldsymbol{b}_l$ and $\boldsymbol{f}_l$ become vectors of length $2m_*+1$, the blocks of $\boldsymbol{A}$ become $(2m_*+1)\times(2m_*+1)$ matrices, and $\boldsymbol{A}$ becomes a $(2m_*+1)N \times (2m_*+1)N$ matrix.

References

1. J. D. Joannopoulos, R. D. Meade and J. N. Winn, *Photonic Crystals: Molding the Flow of Light* (Princeton University Press, Princeton, NJ. 1995).
2. A. Taflove and S. C. Hagness, *Computational electrodynamics : the finite-difference time-domain method*, 3rd ed. (Artech House, Boston, MA. 2005).
3. J. M. Jin, *The finite element method in electromagnetics*, 2nd ed. (John Wiley & Sons, New York, 2002).
4. V. Twersky, "Multiple scattering of radiation by an arbitrary configuration of parallel cylinders," Journal of the Acoustical Society of America **24**, 42-46 (1952).

5. G. O. Olaofe, "Scattering by an arbitrary configuration of parallel circular cylinders," J. Opt. Soc. Am. **60**, 12331236 (1970).
6. D. Felbacq, G. Tayeb and D. Maystre, "Scattering by a random set of parallel cylinders," J. Opt. Soc. Am. A **11**, 2526-2538 (1994).
7. G. Tayeb and D. Maystre, "Rigorous theoretical study of finite-size two-dimensional photonic crystals doped by microcavities," J. Opt. Soc. Am. A **14**, 3323-3332 (1997).
8. J. Yonekura, M. Ikeda and T. Baba, "Analysis of finite 2-D photonic crystals of columns and lightwave devices using the scattering matrix method," J. Lightw. Technol. **17**, 1500-1508 (1999).
9. P. A. Martin, *Multiple Scattering* (Cambridge University Press, Cambridge, UK, 2006).
10. P. Pawliuk and M. Yedlin, "Truncating cylindrical wave modes in two-dimensional multiple scattering," Opt. Lett. **35**, 3997-3999 (2010).
11. R. Borghi, F. Gori, M. Santasiero, F. Frezza, and G. Schettini, "Plane-wave scattering by a set of perfectly conducting circular cylinders in the presence of a plane surface," J. Opt. Soc. Am. A **13**, 2441-2452 (1996).
12. S. C. Lee and J. A. Grzesik, "Light scattering by closely spaced parallel cylinders embedded in a semi-infinite dielectric medium," J. Opt. Soc. Am. A **15**, 163-173 (1998).
13. S. C. Lee, "Light scattering by closely spaced parallel cylinders embedded in a finite dielectric slab," J. Opt. Soc. Am. A **16**, 1350-1361 (1999).
14. A. Coatanhay and J.-M. Conoir, "Scattering near a plane interface using a generalized method of images approach," Journal of Computational Acoustics **12**, 233-256 (2004).
15. F. Frezza, L. Pajewski, C. Ponti, and G. Schettini "Scattering by dielectric circular cylinders in a dielectric slab," J. Opt. Soc. Am. A **27**, 687-695 (2010).
16. Z. Hu and Y. Y. Lu, "Efficient analysis of photonic crystal devices by Dirichlet-to-Neumann maps," Opt. Express **16**, 17383-17399 (2008).
17. Z. Hu and Y. Y. Lu, "Improved Dirichlet-to-Neumann map method for modeling extended photonic crystal devices," Opt. Quant. Electron. **40**, 921-932 (2008).
18. J. Yuan and Y. Y. Lu, "Dirichlet-to-Neumann map method with boundary cells for photonic crystal devices," Communications in Computational Physics, **9**, 113-128 (2011).
19. F. Zolla, R. Petit, and M. Cadilhac, "Electromagnetic theory of diffraction by a system of parallel rods: the method of fictitious sources," J. Opt. Soc. Am. A **11**, 1087-1096 (1994).
20. Y. Huang and Y. Y. Lu, "Scattering from periodic arrays of cylinders by Dirichlet-to-Neumann maps," J. Lightw. Technol. **24**, 3448-3453 (2006).
21. S. Li and Y. Y. Lu, "Computing photonic crystal defect modes by Dirichlet-to-Neumann maps," Opt. Express **15**, 14454-14466 (2007).
22. H. Xie and Y. Y. Lu, "Modeling two-dimensional anisotropic photonic crystals by

Dirichlet-to-Neumann maps," J. Opt. Soc. Am. A **26**, 1606-1614 (2009).

23. Y. Wu and Y. Y. Lu, "Dirichlet-to-Neumann map method for analyzing crossed arrays of circular cylinders," J. Opt. Soc. Am. B **26**, 1984-1993 (2009).
24. S. Li and Y. Y. Lu, "Efficient method for computing leaky modes in two-dimensional photonic crystal waveguides," J. Lightw. Technol. **28**, 978-983 (2010).
25. L. Yuan and Y. Y. Lu, "Dirichlet-to-Neumann map method for analyzing hole arrays in a slab," J. Opt. Soc. Am. B **27**, 2568-2579 (2010).
26. J. Yuan and Y. Y. Lu, "Computing photonic band structures by Dirichlet-to-Neumann maps: The triangular lattice," Opt. Commun. **273**, 114-120 (2007).